RBAV Revista Brasileira de Aplicações de Vácuo
https://doi.org/10.17563/rbav.v45i1.1258
ORIGINAL PAPER

VACUUM COMPONENTS OBTAINED BY SLA 3D PRINTING FOR HIGH-VACUUM APPLICATIONS

Henrique Chaves Gulino[1,*], Ricardo Cardoso Rangel[1], Francisco Tadeu Degasperi[2,3]

1. Universidade de São Paulo – Escola Politécnica – Laboratório de Sistemas Integráveis – São Paulo (SP), Brazil.

2. Faculdade de Tecnologia de São Paulo – Laboratório de Tecnologia do Vácuo – São Paulo (SP), Brazil.

3. Centro Paula Souza – Unidade de Pós-Graduação, Extensão e Pesquisa – São Paulo (SP), Brazil.

Corresponding author: gulino@usp.br

Section Editor: Mariana Fraga

Received: July 27, 2025 **Approved:** Apr. 28, 2026

ABSTRACT

This work presents the development and evaluation of KF-25 standard flanges fabricated by three-dimensional (3D) printing using stereolithography (SLA) for application in high-vacuum systems. The aim was to provide a low-cost, fast, and geometrically flexible alternative to conventional metallic components for laboratory applications. The parts were modeled using Autodesk Inventor and printed with a photopolymer resin on an Anycubic Photon Mono 4K printer. One sample was coated with a 1-μm aluminum layer via thermal evaporation. Optical microscopy revealed continuous surfaces with no visible pores or air pockets, even at the micrometer scale. Pump-down tests were performed using the Edwards Auto 306 vacuum system, in which the original aluminum flange was replaced with the printed samples. Both the untreated and the coated flanges reached final pressures on the order of 10^{-5} mbar. The aluminum-coated sample exhibited improved pressure stability over time, indicating reduced *outgassing*. The results demonstrated that SLA-printed flanges can be effectively used in real high-vacuum conditions, offering significant advantages in terms of fabrication time, cost, and design flexibility. A discussion of the vacuum system and an estimated calculation of its degassing rate are performed. This study provides a promising pathway for future applications in more complex geometries and customized vacuum setups.

KEYWORDS: 3D Printing, Stereolithography, High Vacuum, Vacuum Components, Outgassing.

COMPONENTES DE VÁCUO OBTIDOS POR IMPRESSÃO 3D SLA PARA APLICAÇÕES EM ALTO-VÁCUO

RESUMO

Este trabalho apresenta o desenvolvimento e a avaliação de flanges padrão KF-25 fabricados por impressão tridimensional utilizando a tecnologia de estereolitografia (SLA) para aplicação em sistemas de alto-vácuo. A proposta buscou oferecer uma alternativa de baixo custo, rápida fabricação e alta flexibilidade geométrica para a substituição de componentes metálicos tradicionais em aplicações laboratoriais. As peças foram modeladas no Autodesk Inventor e impressas com resina fotopolimerizável em uma impressora Anycubic Photon Mono 4K. Uma das amostras recebeu um revestimento metálico de alumínio por evaporação térmica, com espessura estimada de 1 μm. A análise morfológica por microscopia óptica revelou superfícies contínuas e sem evidência de poros ou bolsões de ar visíveis, mesmo em escala micrométrica. Os testes de bombeamento foram realizados no sistema Edwards Auto 306, substituindo-se o flange original do equipamento pelas amostras impressas. Os resultados mostraram que tanto a amostra sem tratamento quanto a metalizada atingiram pressões finais da ordem de 10-5 mbar. O revestimento metálico contribuiu para maior estabilidade da pressão ao longo do tempo, reduzindo os efeitos de outgassing. Os dados obtidos demonstram que flanges impressos por SLA podem ser empregados em condições reais de alto-vácuo, oferecendo vantagens em termos de custo, tempo de fabricação e adaptação geométrica. Discussão sobre o sistema de vácuo e o cálculo estimativo da sua taxa de desgaseificação foram realizados. O estudo abre caminho para futuras aplicações em geometrias mais complexas e sistemas customizados de vácuo.

PALAVRAS-CHAVE: Impressão 3D, Estereolitografia, Alto-Vácuo, Componentes de Vácuo, Desgaseificação.

INTRODUCTION

Vacuum technology is widely employed across various stages of product manufacturing and transformation, as well as in fundamental and applied scientific research. Vacuum systems exhibit a wide range of forms and dimensions depending on the pressure, gas type, and flow rate involved[1]. Among the critical components for ensuring system tightness and modularity are flanges, particularly *blank flanges*, which are used for temporary or permanent sealing of open ends. In recent years, additive manufacturing has established itself as a versatile technology for prototyping and fabricating functional parts, including in the field of vacuum technology. However, the application of three-dimensional (3D) printing for components intended for medium and high-vacuum environments still faces significant limitations, mainly related to gas permeability and the outgassing behavior of polymeric materials[2,3].

Recent advances include the study by Rangel et al.[2], who evaluated KF-25 flanges fabricated via fused filament fabrication 3D printing using polylactic acid (PLA). By implementing unidirectional printing, polishing, and aluminum coating, they enhanced the vacuum performance of the printed parts, achieving final pressures on the order of 6×10^{-1} mbar still restricted to low-vacuum applications. Complementarily, Chanelière[3] showed that acrylonitrile butadiene styrene (abs)-printed flanges fabricated with entry-level 3D printers can reach pressures near 10^{-5} mbar when coated with Vacseal varnish and subjected to bake-out, highlighting the role of post-processing in improving vacuum compatibility.

Despite these advancements, only recently a few studies have begun to explore the use of stereolithography (SLA) 3D printing for manufacturing vacuum components, highlighting the potential of these materials when appropriately treated to mitigate outgassing effects[4,5]. However, systematic studies evaluating SLA-printed blank flanges specifically intended for high-vacuum applications remain scarce.

In this context, the present work proposed the fabrication of KF-25 flanges using SLA 3D printing, aiming to assess their viability in high-vacuum conditions (10^{-3} to 10^{-5} mbar). One of the printed flanges was coated with a thin aluminum film via physical vapor deposition (PVD) using thermal evaporation, to evaluate the influence of surface treatment on vacuum performance. The samples were integrated into a high-vacuum pumping system, and the ability to reach pressures around 1×10^{-5} mbar was assessed, along with the subsequent pressure rise behavior. All results were compared to a commercial aluminum KF-25 flange used as reference.

METHODS

This section describes the procedures adopted for the fabrication, surface treatment, and characterization of *blank flanges* produced via SLA 3D printing, with the aim of evaluating their performance in high-vacuum systems. The stages of part modeling and printing, post-curing, PVD, and the experimental protocol for vacuum pumping and pressure measurement were thoroughly documented.

To assess the performance of the printed flanges under high-vacuum conditions, comparative tests were conducted between three distinct configurations: one SLA flange without any additional treatment, a second sample coated with an aluminum thin film deposited by thermal evaporation, and a commercial aluminum KF-25 flange used as a reference. All samples were subjected to the same assembly and measurement procedures in a vacuum system equipped with instrumentation suitable for monitoring pressure in the 10^{-5} mbar range.

Project and fabrication

The blank flanges were designed according to the KF-25 standard using Autodesk Inventor CAD software. Fabrication was carried out via SLA 3D printing using the Anycubic Photon Mono 4K printer. The printing material was standard resin, a photopolymer widely used for technical prototyping applications. Both the printer and the resin are commercially available at low cost, making this approach attractive for academic and low-budget laboratory settings. Figure 1 shows the printer and resin used during the work.

Figure 1: Stereolithography three-dimensional printer (Anycubic Photon Mono 4K) and standard resin used for the fabrication of KF blank flanges.

Source: Adapted from Anycubic[6,7].

Print preparation was performed using Chitubox software, which provided estimates for print time, material volume, and exposure parameters. The flanges were printed in a horizontal orientation to reduce total fabrication time. This setup required fewer layers, which significantly accelerated the process without notably compromising the dimensional quality of the sealing surface. The results confirmed the high efficiency of the method: each flange required only 1.03 mL of resin and 7 minutes and 33 seconds to print. This represents both a very low material consumption and an extremely short build time, making the process well-suited for rapid prototyping and low-cost experimental runs.

Figure 2 shows the flange geometry, printing parameters, and estimated values for volume (1.03 mL), weight (1.1 g), and total print time. The main print settings used were layer height of 0.05 mm, exposure time of 2 seconds per layer, bottom exposure time of 10 seconds, lifting speed of 120 mm/min, retraction speed of 180 mm/min, and lift distance of 1.5 mm. After printing, the flanges were washed in isopropyl alcohol (IPA) to remove uncured resin. They were then post-cured in an ultraviolet chamber following the resin manufacturer's specifications, ensuring full polymer crosslinking and stabilization of mechanical properties.

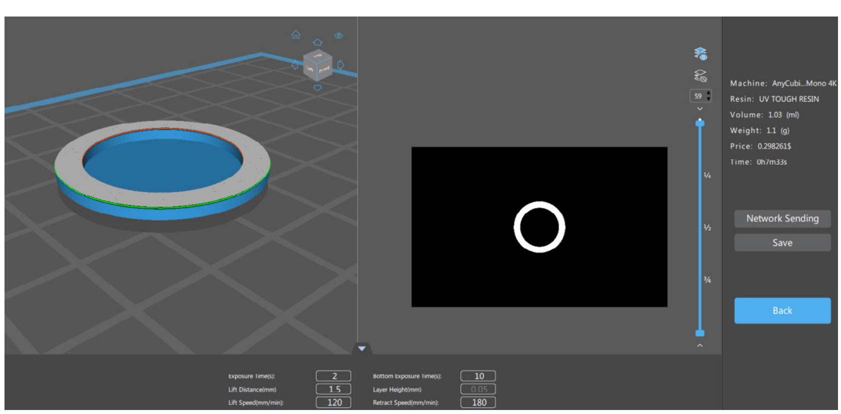

Figure 2: Slicer interface in Chitubox showing the KF-25 blank flange geometry, printing parameters, and estimated values for print time, material volume, and part weight.

Source: Elaborated by the authors.

Figure 3 illustrates the fabrication workflow of KF-25 blank flanges using SLA 3D printing, from digital modeling to post-curing. The process comprises the following steps:

- 3D modeling (Fig 3a): The flange was designed using Autodesk Inventor, following the dimensional specifications and tolerances of the KF-25 standard. The model includes the central circular aperture and sealing rim, both critical to ensure proper fit and vacuum tightness;
- Print setup and slicing in Chitubox (Fig 3b): The 3D model was imported into Chitubox slicing software and placed horizontally on the build platform. Key parameters such as layer height, exposure time, and lift/retraction speeds were defined. The bottom image in Fig. 3b shows a slice preview, highlighting the distribution of the exposed resin layer during the photopolymerization process;
- Part after washing (Fig 3c): Once printed, the flange was detached from the build plate and washed with IPA to remove residual uncured resin. This step is essential to prevent contamination during post-curing and to maintain the dimensional precision of the sealing region;
- Ultraviolet post-curing (Fig 3d): The part underwent post-curing in an ultraviolet chamber to ensure full polymer crosslinking. This treatment improves the part's mechanical strength, dimensional stability, and overall suitability for vacuum applications.

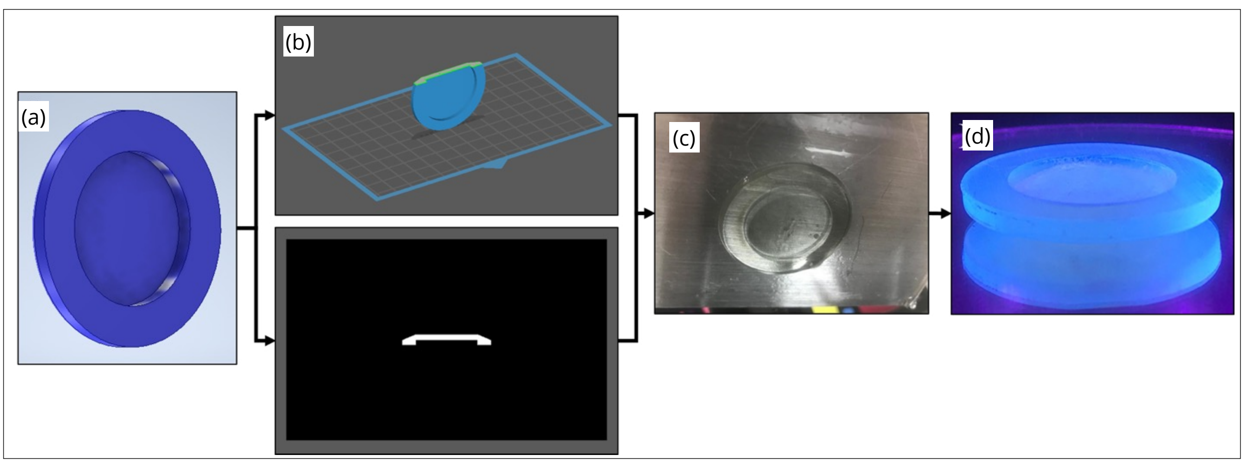

Figure 3: Full flowchart.

Source: Elaborated by the authors.

To investigate potential improvements in vacuum performance, one of the printed flanges was subjected to surface treatment via PVD using thermal evaporation. A thin aluminum layer with an estimated thickness of approximately 1 μm was deposited to reduce gas permeability and the inherent outgassing rate of the polymeric substrate. Aluminum was chosen due to its well-established properties in vacuum technology: high thermal conductivity, good adhesion to various substrates, low outgassing after proper bake-out, and ease of deposition via thermal evaporation. Additionally, the metallic coating may act as a partial diffusion barrier, limiting the migration of volatile organic species from the bulk material to the surface.

The deposition was carried out in an Edwards Auto 306 thermal evaporator, operating at a base pressure below 1×10^{-5} mbar, with thickness monitored via quartz crystal microbalance. The sample was positioned to ensure uniform coverage of the sealing surface and the external face of the flange. Morphological characterization of the printed flanges was performed using optical microscopy with a Karl Zeiss Jeneval microscope. This inspection provided qualitative assessment of the surface, focusing on residual roughness, defects, and any discontinuities in the sealing region all of which are critical for vacuum system performance. Vacuum testing was carried out using the Edwards Auto 306 (Figs. 4 and 5) thermal evaporation system, which is conventionally used for PVD processes. The high-vacuum system, with a final pressure of 1×10^{-5} mbar, consists of a bell-shaped glass vacuum chamber. Connected to the vacuum chamber is a diffusion pump with a cold trap (liquid nitrogen) and a baffle. The diffusion pump is a Diffstak™ type (with a baffle incorporated directly into the diffusion pump). The pre-vacuum pump is a mechanical vane type. There are Pirani pre-vacuum gauge and Penning high-vacuum gauge. The vacuum system is sufficient for the final pressure determination work, considering the polymeric flange under test. The vacuum is broken in the vacuum chamber with atmospheric air.

The test adopted a practical approach: the system's original aluminum flange was removed and replaced with one of the printed flanges, keeping all other operational parameters unchanged. This allowed direct evaluation of the printed component's influence on vacuum pump-down behavior and final pressure. Comparison with the reference flange enabled validation of sealing integrity, assessment of outgassing effects, and verification of the feasibility of using polymer-based flanges in high-vacuum systems under real operating conditions.

Figure 4: System used for vacuum testing. At the top, an overview of the Edwards Auto 306 system with the test flange installed. On the left, detail of the replacement of the original flange with a printed sample.

Source: Elaborated by the authors.

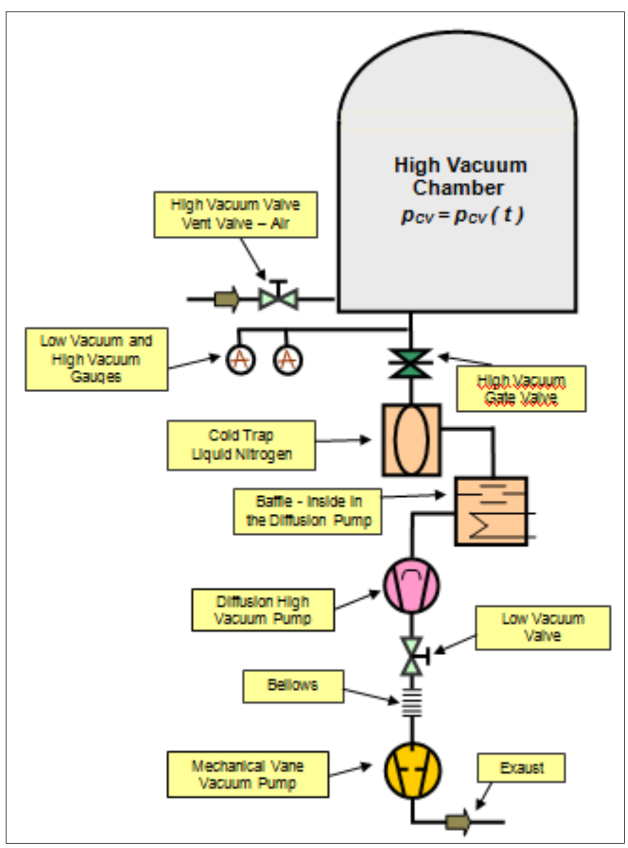

Figure 5: Vacuum system schematic diagram of the vacuum line, highlighting the main components: mechanical pump, DiffstakTM diffusion pump (with baffle inside in the diffusion pump), cold trap, isolation valves, and purge line.

Source: Elaborated by the authors.

RESULTS AND DISCUSSION

This section presents and discusses the main results obtained from the morphological analysis of the printed flanges, as well as from the high-vacuum compatibility tests. The data allow for evaluating the impact of the chosen fabrication method, the presence of surface treatments, and the material type on the performance of the components under real-vacuum pumping conditions.

The discussion begins with observations made via optical microscopy on the flange surfaces, aiming to identify porosity, discontinuities, or surface roughness that could compromise sealing performance. Subsequently, experimental results obtained from tests carried out in the Edwards Auto 306 system are presented, with emphasis on pump-down curves and the minimum pressure achieved. The effect of the aluminum coating is also analyzed, allowing for comparison between treated and untreated flanges. Finally, the results are contrasted with those obtained using a commercial aluminum KF-25 flange, which served as a reference.

Morphological analysis

Morphological characterization (Fig. 6) of the printed flanges was performed using optical microscopy with a Karl Zeiss Jeneval microscope equipped with a digital camera and 10x to 50x objective lenses. Prior to the analysis, the samples were prepared by washing them in IPA to remove uncured resin and post-cured in an ultraviolet chamber to ensure full polymer crosslinking, with no additional surface polishing applied before microscopic inspection. This inspection provided qualitative assessment of the surface, focusing on residual roughness, defects, and any discontinuities in the sealing region all of which are critical for vacuum system performance.

- At lower magnification (100-µm scale), regular layer marks from the slicing process are observed in a cross-hatched pattern, with no evidence of open pores or structural discontinuities. The even distribution of cured layers and the absence of delamination suggest good interlayer adhesion during printing;
- At intermediate magnification (10-µm scale), the surface still appears uniform, with no visible air pockets or voids, indicating a dense and well-polymerized matrix. The subtle texture is likely due to photopolymerization fronts between cured zones;
- At higher magnification, the surface displays smooth microtextures and no signs of cavities or aggregated defects, further supporting the high quality of the SLA surface finish. The absence of visible defects at this resolution also confirms that the optical system's pixel size (~10 µm) is sufficient for reliable assessment.

Taken together, the results confirmed that the printed surfaces are continuous, pore-free, and of high integrity, making them suitable for vacuum sealing applications. The surface uniformity also suggests that the printing and post-curing parameters effectively ensured homogeneous curing.

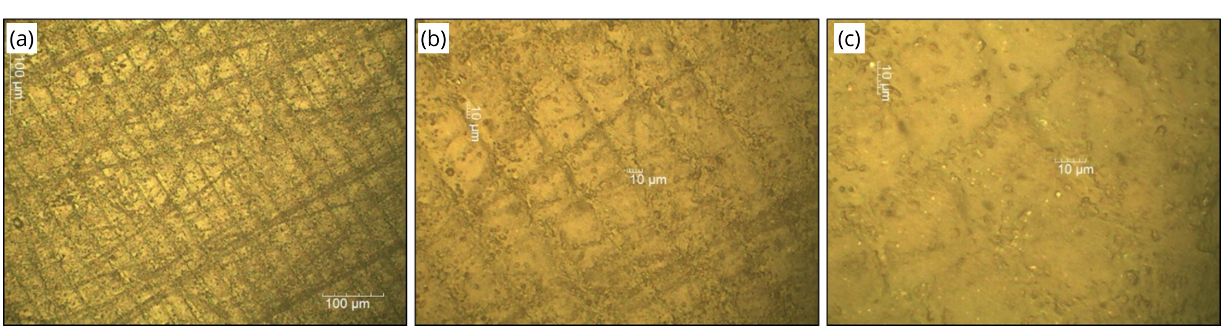

Figure 6: Optical micrographs of the stereolithography-printed flange surface at different magnifications: (a) 100 µm, (b) 10 µm, and (c) 10 µm. No visible porosity or surface defects were observed.

Source: Elaborated by the authors.

Vacuum performance

Figure 7 presents pressure *versus* time pump-down curves for three KF-25 flange configurations: commercial aluminum flange, SLA-printed resin flange with aluminum PVD coating, and SLA-printed resin flange without coating. All samples displayed similar behavior during the initial evacuation stage, reaching high-vacuum levels (pressures below 1×10^{-4} mbar) within approximately 300 seconds. From this point, the system entered a stabilization regime. The commercial aluminum flange performed consistently and served as a reference. The resin flange with aluminum coating closely followed the performance of the commercial sample, reaching final pressures around 1×10^{-5} mbar, indicating good sealing, low outgassing, and compatibility with high-vacuum applications. The uncoated resin flange exhibited slightly higher final pressures, but still achieved values in the 10-5 mbar range, demonstrating that the printing and post-curing process alone ensured adequate performance, even without metallization. The observed performance improvement in the coated sample confirmed the beneficial effect of the aluminum layer, which likely acts as a diffusion barrier, reducing gas permeation and contributing to vacuum stability over time.

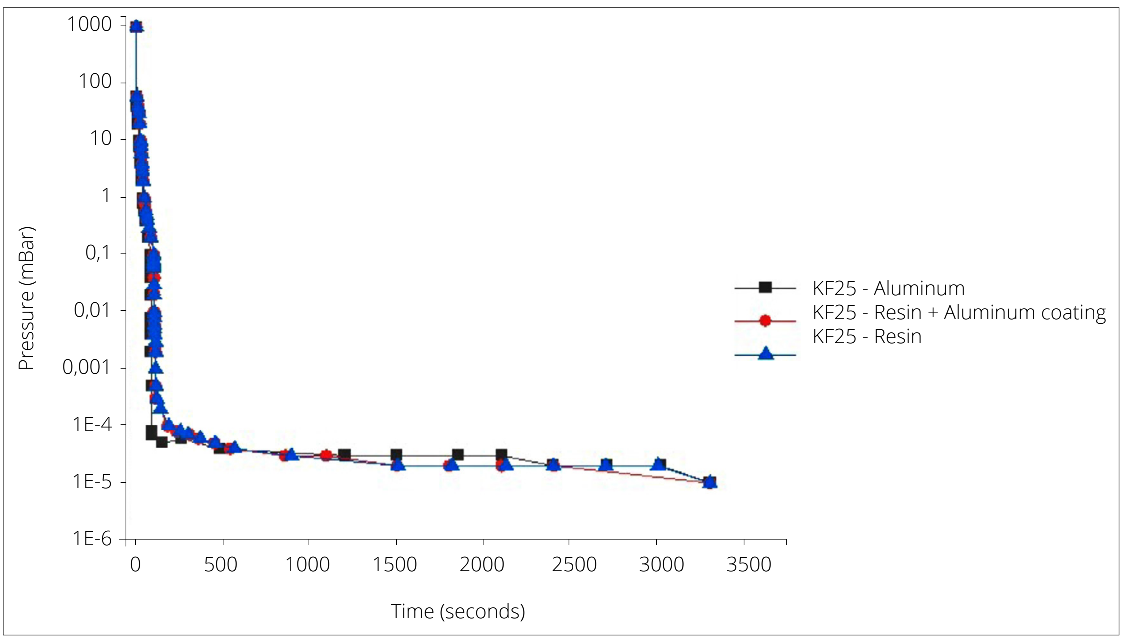

Figure 7: Pump-down curves for different KF-25 flanges: commercial aluminum flange, stereolithography-printed resin flange with aluminum coating, and uncoated resin flange. Metallization slightly improves performance, approaching the reference behavior.

Source: Elaborated by the authors.

After reaching the minimum pressure, the system was isolated and the pressure rise over time was monitored, as shown in Fig. 8. This test assesses the rate of pressure increase due to material *outgassing*, permeation, or possible leaks. The commercial aluminum flange showed the most stable behavior, with pressure remaining below 0.02 mbar even after 1,500 seconds, confirming its excellent performance in high-vacuum environments. The resin flange with aluminum coating displayed moderate pressure increase, indicating that the metallic layer contributes positively by limiting the release of volatiles from the polymer matrix.

The uncoated resin flange showed the highest-pressure increase, exceeding 0.1 mbar by the end of the measurement. This behavior is typical for untreated polymers due to residual outgassing, but it still demonstrates that the component remains functional for short-term high-vacuum use particularly in scenarios in which maintaining extreme vacuum is not critical over time. These findings are consistent with the pump-down results and reinforce the barrier effect of the aluminum coating against surface outgassing.

To calculate the approximate degassing rate of the vacuum chamber and its support plate, one must consider the final pressure reached by the high-vacuum system and the effective pumping speed at the vacuum chamber entrance. The differential equation that determines the pressure evolution in the vacuum chamber is shown in Eq. 1.

$$V_{CV}\,\frac{dp_{CV}(t)}{dt} = -S_{ef}\,p_{CV}(t) + \sum_{i=1}^{n} Q_i \Rightarrow V_{CV}\,\frac{dp_{CV}(t)}{dt} = -S_{ef}\,p_{CV}(t) + Q_{outog} \quad (1)$$

where: V_{CV}: the volume of the vacuum chamber; $p_{CV}(t)$: the pressure in the vacuum chamber, which depends on time; S_{ef}: the effective pumping speed, with dependent on the pumping speed of the diffusion pump, the pumping speed of the ice trap for gaseous water, and the conductance of the pumping line (valve, pipes and cold trap).

It is necessary to consider that of all the possible sources of gases that may be present in the vacuum system, only outgassing will be considered, which is due to the gas released by surfaces exposed to high vacuum (Eq. 2):

$$-S_{ef}\,p_{CV}^{final} + Q_{outog} = 0 \Rightarrow Q_{outg} = S_{ef}\,p_{CV}^{final} \quad (2)$$

Assuming, through a quick calculation, that the effective pumping speed is 200 $L{\cdot}s^{-1}$, and the measured vacuum chamber pressure is 1×10^{-5} mbar, the total outgassing rate of the vacuum system is obtained (Eq. 3).

$$Q_{outg} = 200 \times 10^{-5} \Rightarrow Q_{outg} = 2 \times 10^{-3}\ \mathrm{mbar.L.s^{-1}} \quad (3)$$

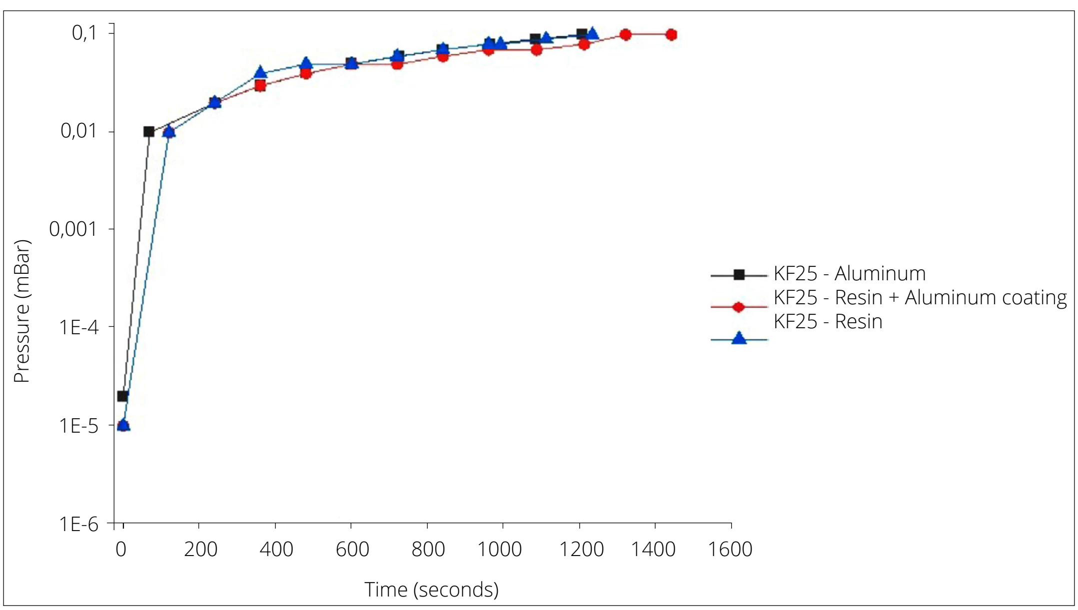

Figure 8: Pressure rise over time after pump shutoff for different KF-25 flanges. The metallic sample exhibits the lowest outgassing, while the uncoated resin flange shows the highest-pressure variation.

Source: Elaborated by the authors.

CONCLUSION

This study demonstrated the feasibility of using KF-25 standard flanges fabricated via SLA 3D printing for high-vacuum applications. The results highlight several advantages of this approach, both technically and logistically. The components were fabricated in extremely short time frames (less than 10 minutes per unit) with minimal material consumption (≈ 1 mL of resin), using low-cost, readily available equipment and supplies. This makes the method particularly attractive for academic and applied research environments, in which rapid and flexible prototyping is essential.

Moreover, additive manufacturing enables the production of non-standard geometries that, in conventional methods, would require complex machining, welding, or multi-part assembly. Morphological analysis revealed continuous, pore-free surfaces, even at magnifications down to 10 μm, ensuring sealing integrity for vacuum use. The absence of structural defects confirms the effectiveness of the printing and post-curing procedures. Vacuum testing showed that even untreated SLA-printed flanges achieved final pressures in the 10-5 mbar range.

The application of an aluminum coating via thermal evaporation slightly improved pump-down performance and significantly enhanced pressure stability over time. In both cases, the results closely matched those of a commercial aluminum flange, confirming the viability of this solution. Future work may explore alternative printing resins with lower gas permeability, the implementation of higher-temperature bake-out procedures, and the integration of sealing features directly into printed parts. The methodology could also be extended to more complex geometries and validated across a broader range of vacuum applications, including thin-film deposition, spectroscopy, and controlled-atmosphere experiments.

Considering the progress made in the construction of parts using 3D printing of the polymeric material used in this work, a more detailed study is warranted, with a possible application in cases in which a replacement part is required to be manufactured on-site for the vacuum system. A polymeric part is considered a temporary, quickly constructed replacement. Consideration should also be given to the construction of parts in locations in which metal workshops are not available, such as on space stations, in which this type of construction becomes a viable and simple alternative.

Next steps

To consider limits for the use of parts manufactured with the polymer used in this work, surfaces with sufficiently large areas should be considered so that the degassing rate and permeation rate of these materials can be determined experimentally. A study on the dependence of these quantities on the thickness of the material used should also be conducted. Thus, the safe use of the polymer under study may be considered as an alternative for certain vacuum and high-vacuum systems.

CONFLICT OF INTEREST

Nothing to declare.

AUTHOR CONTRIBUTIONS

Conceptualization: Gulino HC; **Formal Analysis:** Gulino HC, Rangel RC and Degasperi FT; **Investigation:** Gulino HC, Rangel RC and Degasperi FT; **Resources:** Gulino HC; **Supervision:** Rangel RC and Degasperi FT; **Validation:** Gulino HC; **Data curation:** Gulino HC, Rangel RC and Degasperi FT; **Writing – first draft:** Gulino HC; **Writing – review and editing:** Gulino HC, Rangel RC and Degasperi FT; **Final approval:** Gulino HC.

DATA AVAILABILITY STATEMENT

All dataset were generated or analyzed in the current study.

FUNDING

Coordenação de Aperfeiçoamento de Pessoal de Nível Superior
Finance code 001

DECLARATION OF USE OF INTELLIGENCE ARTIFICIAL TOOLS

The authors declare that no artificial intelligence tools were used in the preparation, writing, data analysis, or review of this manuscript.

ACKNOWLEDGEMENTS

The authors thank the Laboratório de Sistemas Integráveis of the Escola Politécnica of the Universidade de São Paulo and the Laboratório de Tecnologia do Vácuo of the Faculdade de Tecnologia de São Paulo/Centro Estadual de Educação Tecnológica Paula Souza for providing the infrastructure used during the development of this work.

REFERENCES

1. Degasperi FT. Modelagem e análise detalhadas de sistemas de vácuo [Dissertation, Faculdade de Engenharia Elétrica e de Computação, Universidade Estadual de Campinas]. https://doi.org/20.500.12733/1593241

2. Rangel RC, Gulino HC, Degasperi FT. Vacuum components obtained by 3D printing using biodegradable plastic. RBAV. 2024;43:e0124. https://doi.org/10.17563/rbav.v43i1.1246

3. Chanelière T. Vacuum compatibility of ABS plastics 3D-printed objects. CNRS, Laboratoire Aimé Cotton; 2017 [cited 2026 Apr 30]. Available at: https://hal.science/hal-01599113

4. Radić A, Lambrick SM, Rhodes S, Ward DJ. On the application of components manufactured with stereolithographic 3D printing in high vacuum systems. Vacuum. 2025;232:113809. https://doi.org/10.1016/j.vacuum.2024.113809

5. Kumar V, Lausti NV, Hajnys J, Hudák I, Motycka D, Jelínek A, Hejduk M. 3D-printed components for electron-ion trapping: Tests of functionality and ultra-high vacuum compatibility. arXiv. 2025;2509.06537. https://doi.org/10.48550/arXiv.2509.06537

6. Anycubic. Anycubic photon mono 4K. Anycubic [cited 2025 July 24]. Available at: https://store.anycubic.com/products/photon-mono-4k

7. Anycubic. Standard resin. Anycubic [cited 2025 July 24]. Available at: https://store.anycubic.com/products/colored-uv-resin